Electronic Supplementary Material (ESI) for Environmental Science: Nano.

Effective strategies toward imine-linked cationic covalent organic frameworks for rapid and selective removal of $^{99}TcO_4^-$ from water: Insights from DFT and MD calculations

Chaofeng Zhao[†], Xinjie Ma[†], Xin Wei[§], Weiwei Liu[‡], Lu Sun[*,‡], Yuejie Ai[*,†]

[†] *MOE Key Laboratory of Resources and Environmental Systems Optimization, College of Environmental Science and Engineering, North China Electric Power University, Beijing 102206, P. R. China*

[‡] *Institute of Modern Optics, Tianjin Key Laboratory of Micro-scale Optical Information Science and Technology, Nankai University, Tianjin, 300350, P. R. China*

[§] *School of Control and Computer Engineering, North China Electric Power University, Beijing 102206, P. R. China*

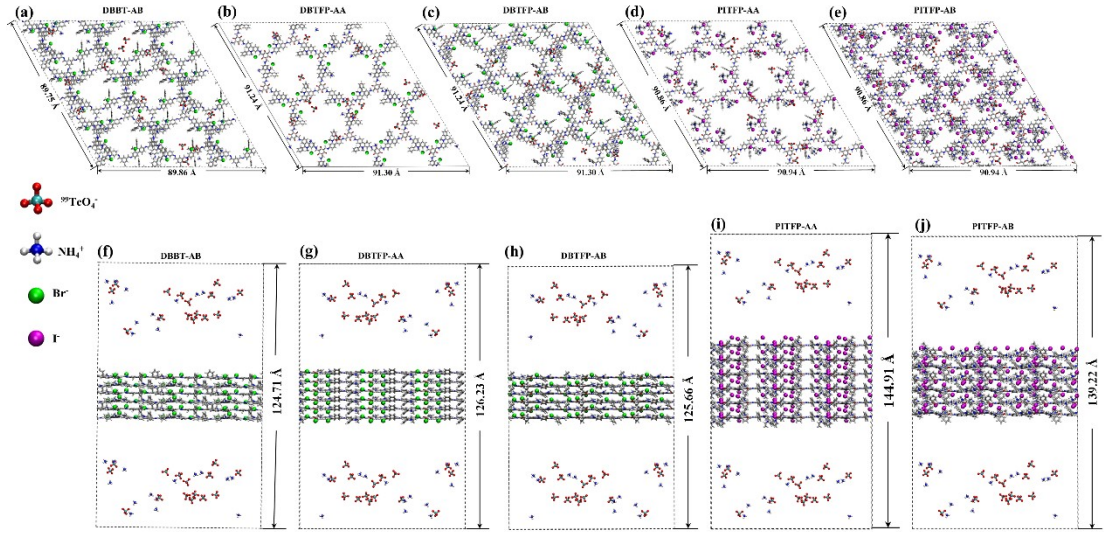

Fig. S1. The top views (a-e) and side views (f-j) of the initial configurations for the MD simulated DBBT-AB, DBTFP-AA, DBTFP-AB, PITFP-AA and PITFP-AB systems under the LC condition. All cationic COFs are displayed as licorice style and water molecules are hidden to clarify the position of other molecules.

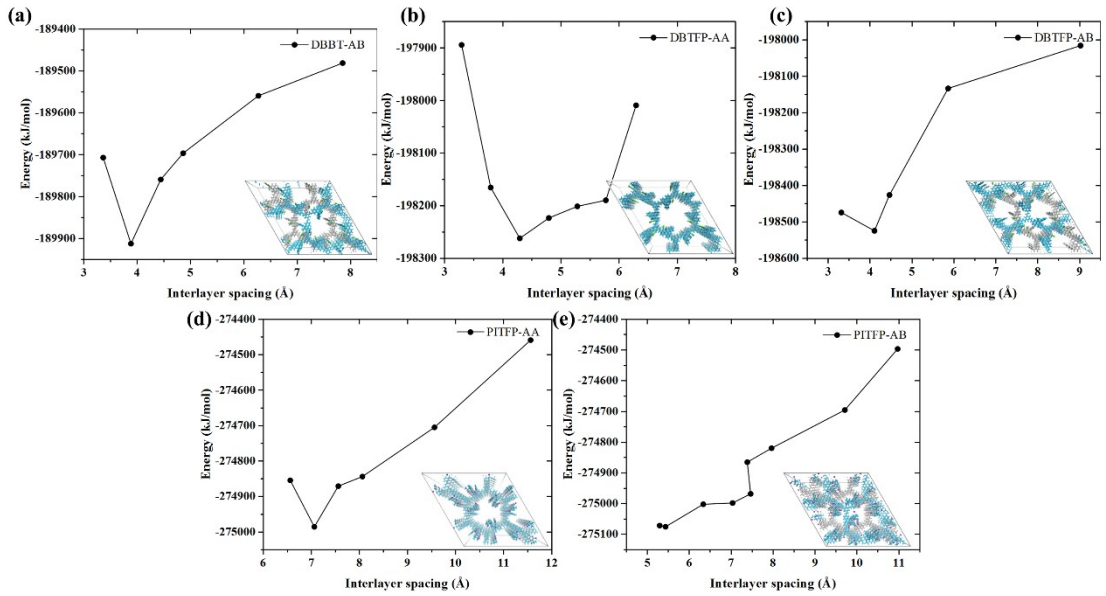

Fig. S2. The energies of (a) DBBT-AB, (b) DBTFP-AA, (c) DBTFP-AB, (d) PITFP-AA, (e) PITFP-AB in different interlayer distances together with the optimal structures.

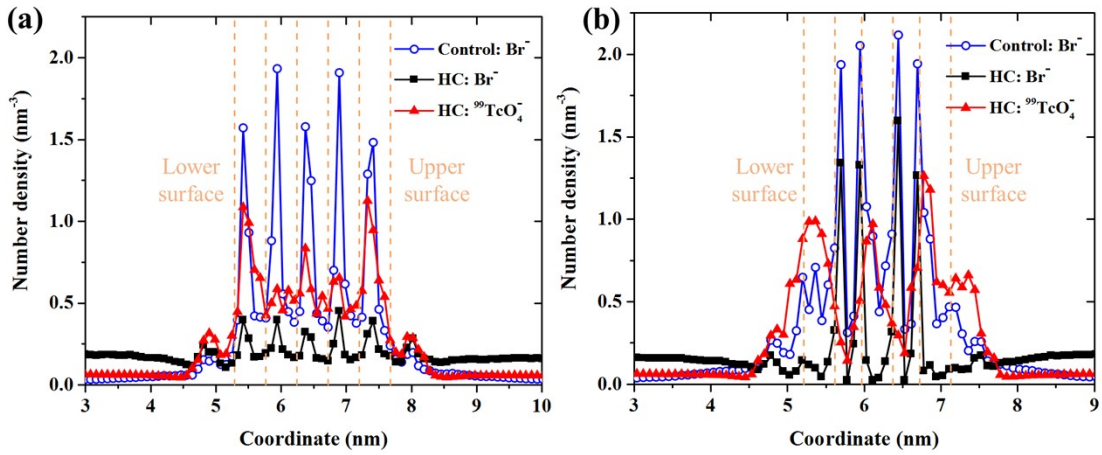

Fig. S3. The number densities of Br^- and $^{99}TcO_4^-$ in (a) DBBT-AA and (b) DBBT-AB under the HC condition together with the data of Br^- in the control group. The orange dashed lines show the location of each layer.

As for the HC condition in Fig. S3, in addition to the booming amount, more $^{99}TcO_4^-$ prefer to locate at the lower and upper surfaces of DBBT with large proportions. From the distributions of remaining Br^- in DBBT, Br^- ions near the surfaces are almost completely desorbed but it in inner layers are difficult to desorb. Combined with the self-exfoliated feature of cationic COFs,[1] we can conclude that the fewer layer of DBBT is more efficient in practical application for $^{99}TcO_4^-$ elimination.

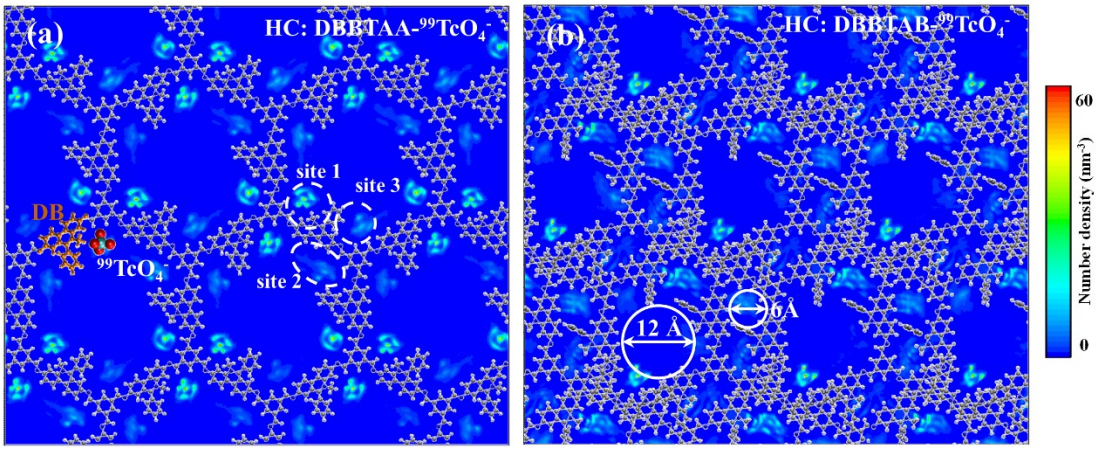

Fig. S4. The 2D number density distributions of $^{99}TcO_4^-$ in (a) DBBT-AA and (b) DBBT-AB under the HC condition.

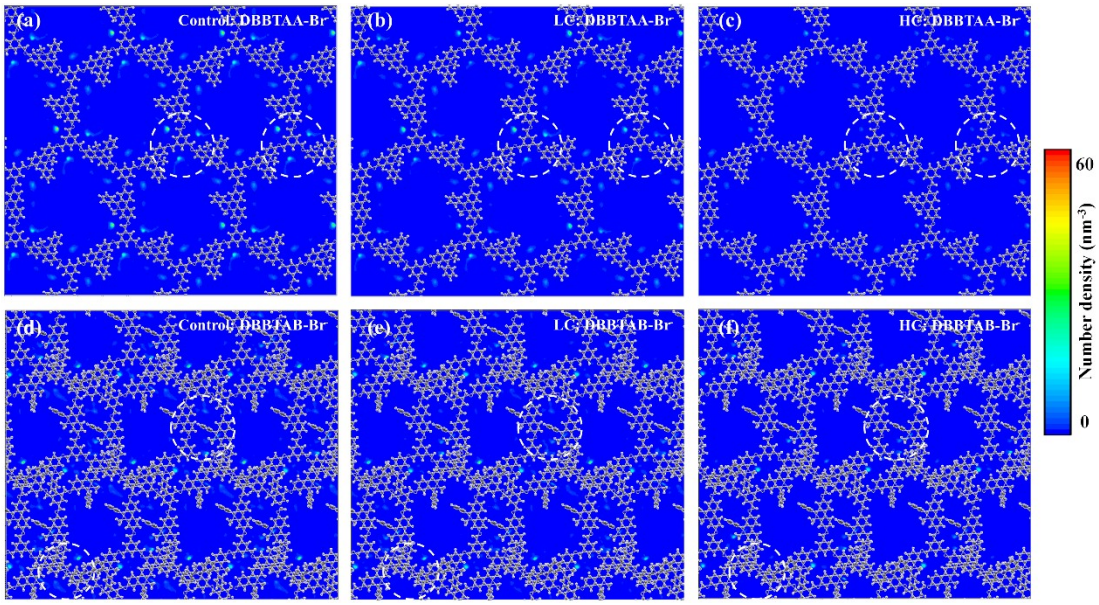

Fig. S5. The 2D number density distributions of remaining Br^- in DBBT-AA (a-c) and DBBT-AB (d-f) under the control group, LC and HC conditions, respectively.

From Fig. S5, the 2D number density distributions of the remaining Br^- in DBBT-AA and DBBT-AB under each condition show that decreasing number densities of Br^- is associated with the increased adsorption of $^{99}TcO_4^-$ near the anion binding sites, indicating effective anion-exchange process between them.

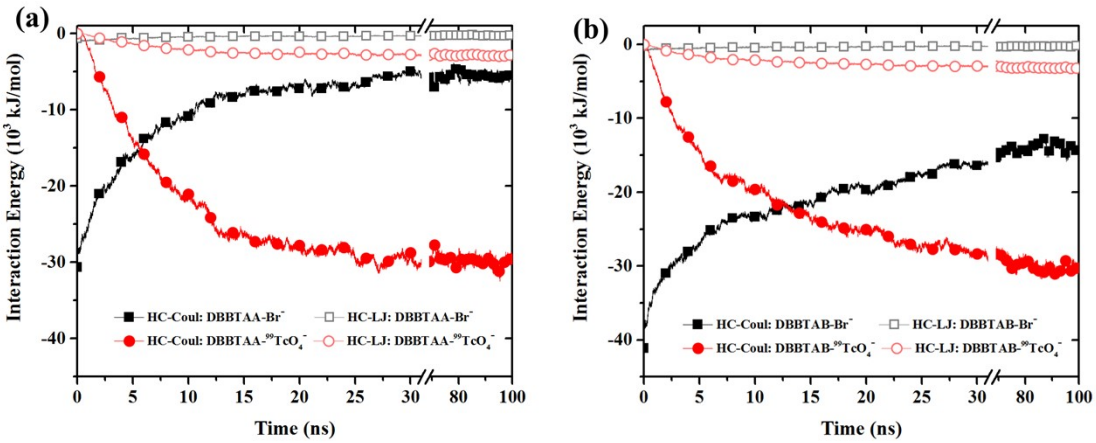

Fig. S6. The Coulomb interaction energies and LJ potentials between (a) DBBT-AA as well as (b) DBBT-AB and anions at HC condition.

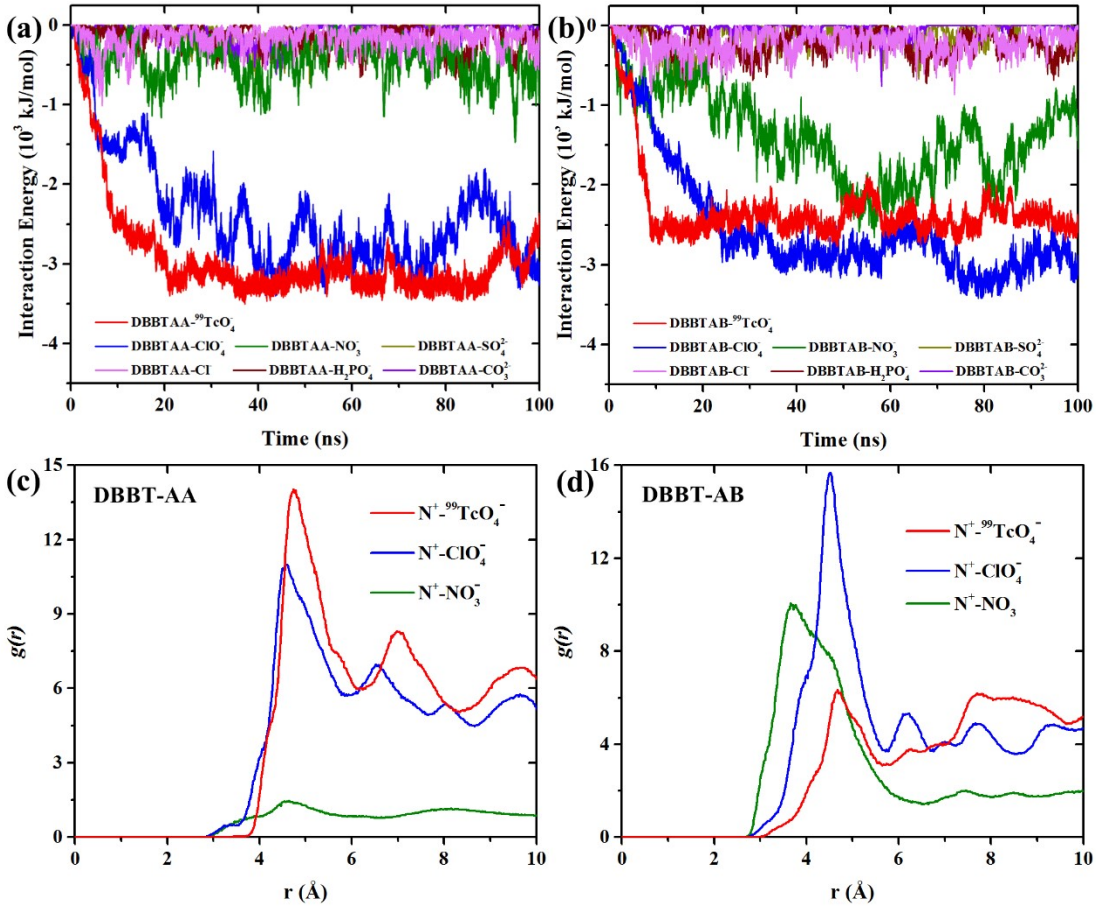

Fig. S7. The Coulomb interaction energies between (a) DBBT-AA as well as (b) DBBT-AB and anions. The radial distribution functions of $^{99}TcO_4^-$, ClO_4^- and NO_3^- near the positively charged nitrogen atoms in (c) DBBT-AA and (d) DBBT-AB.

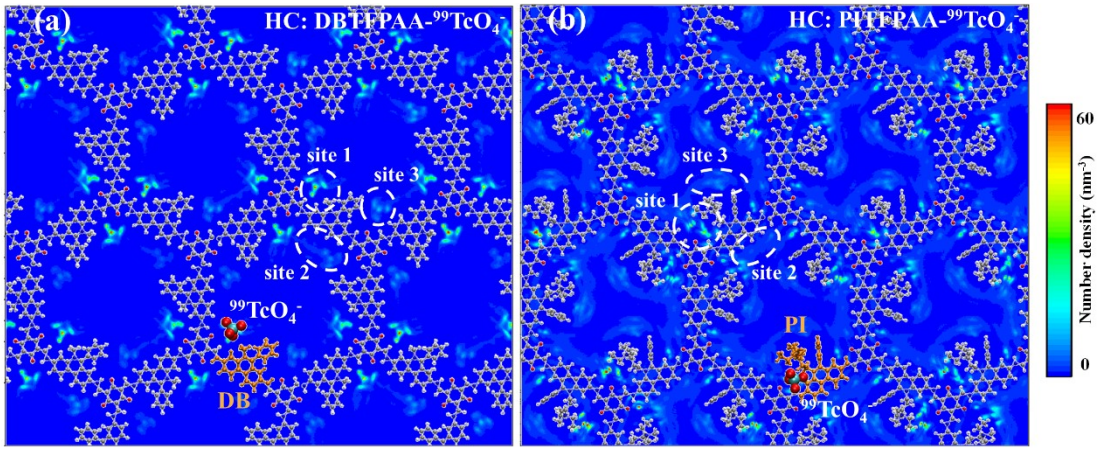

Fig. S8. The 2D number density distributions of $^{99}TcO_4^-$ in (a) DBTFP-AA and (b) PITFP-AA under the HC condition.

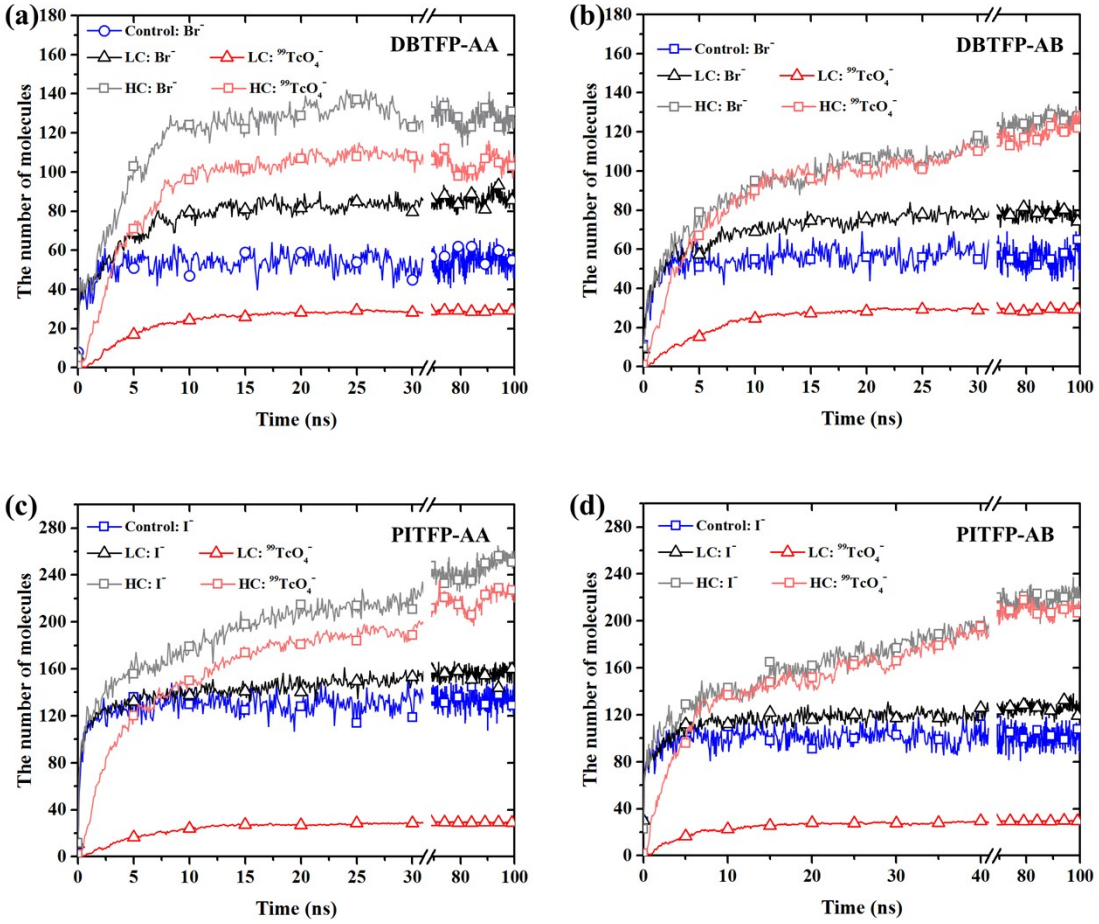

Fig. S9. Time evolution of the amounts of desorbed Br^- (or I^-) and adsorbed $^{99}TcO_4^-$ in (a) DBTFP-AA, (b) DBTFP-AB, (c) PITFP-AA and (d) PITFP-AB under different conditions.

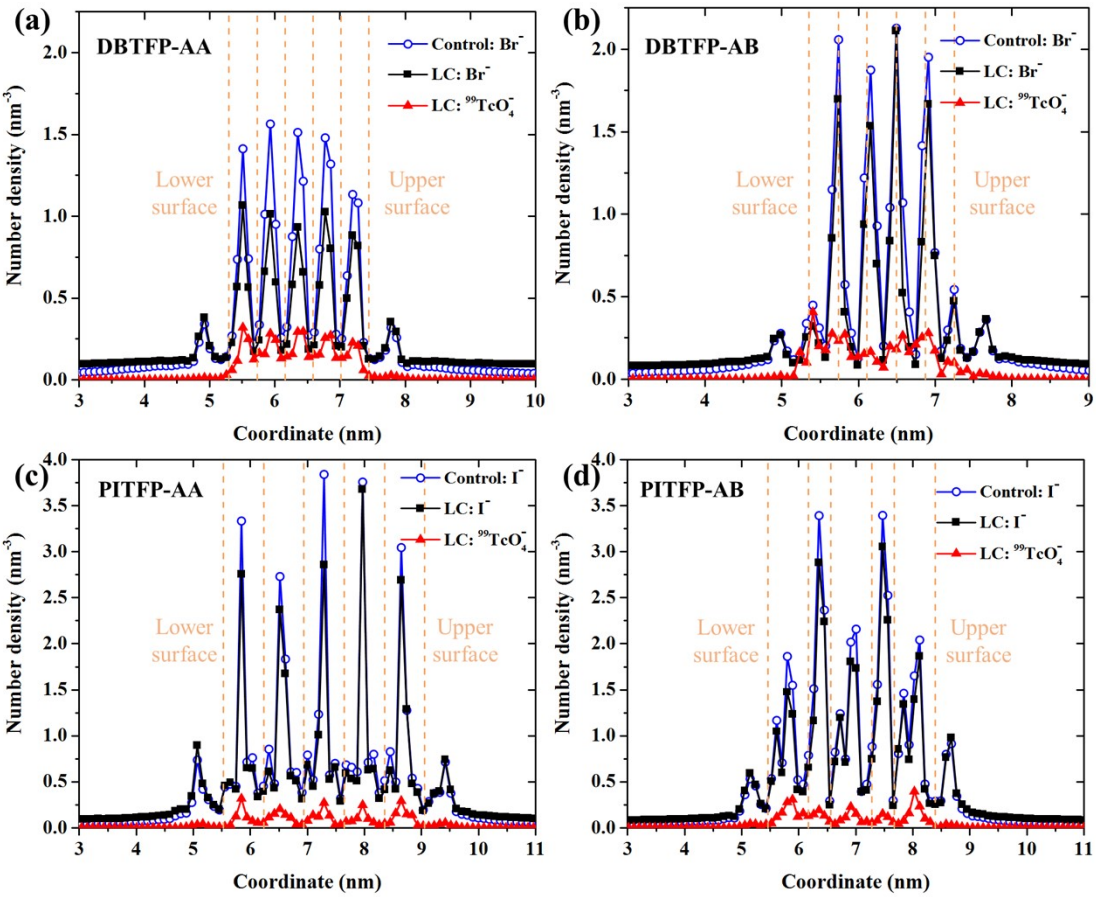

Fig. S10. The number densities of Br^- (or I^-) and $^{99}TcO_4^-$ in (a) DBTFP-AA, (b) DBTFP-AB, (c) PITFP-AA and (d) PITFP-AB under LC condition together with the data of Br^- (or I^-) in the control group. The orange dashed lines show the location of each layer.

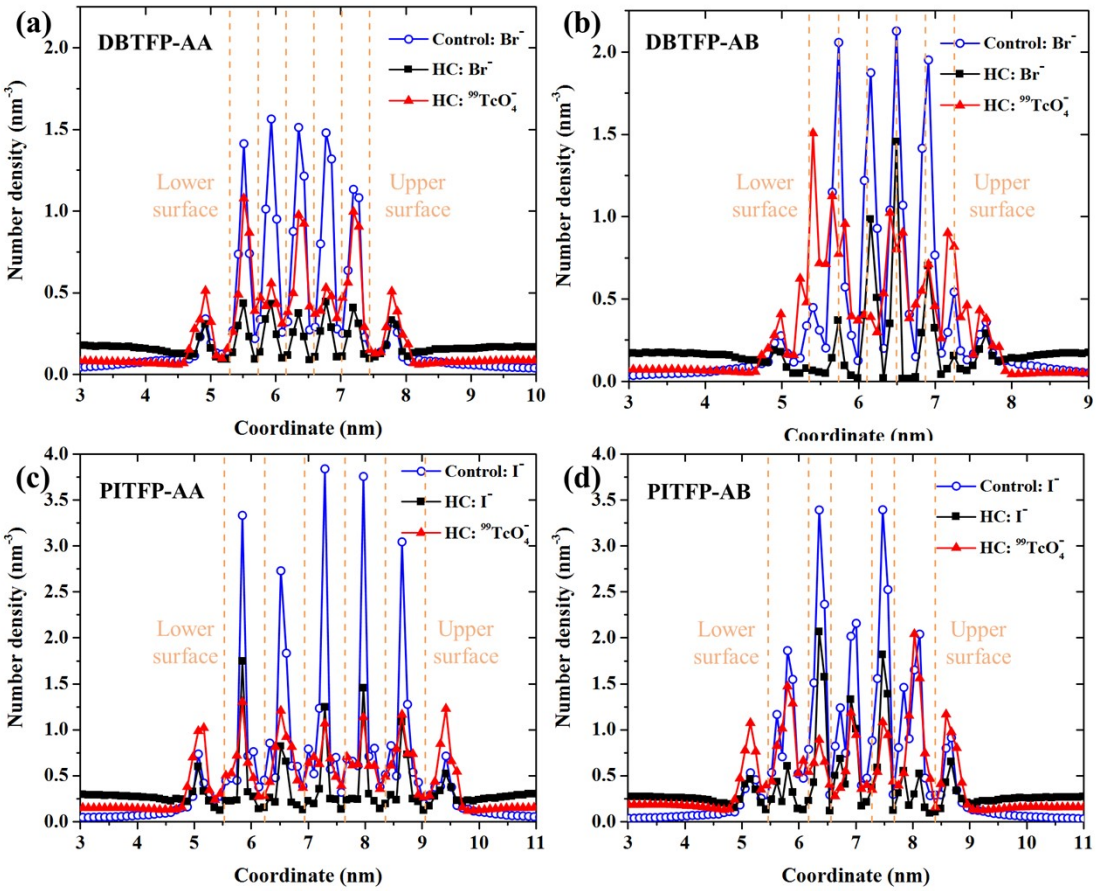

Fig. S11. The number densities of Br^- (or I^-) and $^{99}TcO_4^-$ in (a) DBTFP-AA, (b) DBTFP-AB, (c) PITFP-AA and (d) PITFP-AB under HC condition together with the data of Br^- (or I^-) in the control group. The orange dashed lines show the location of each layer.

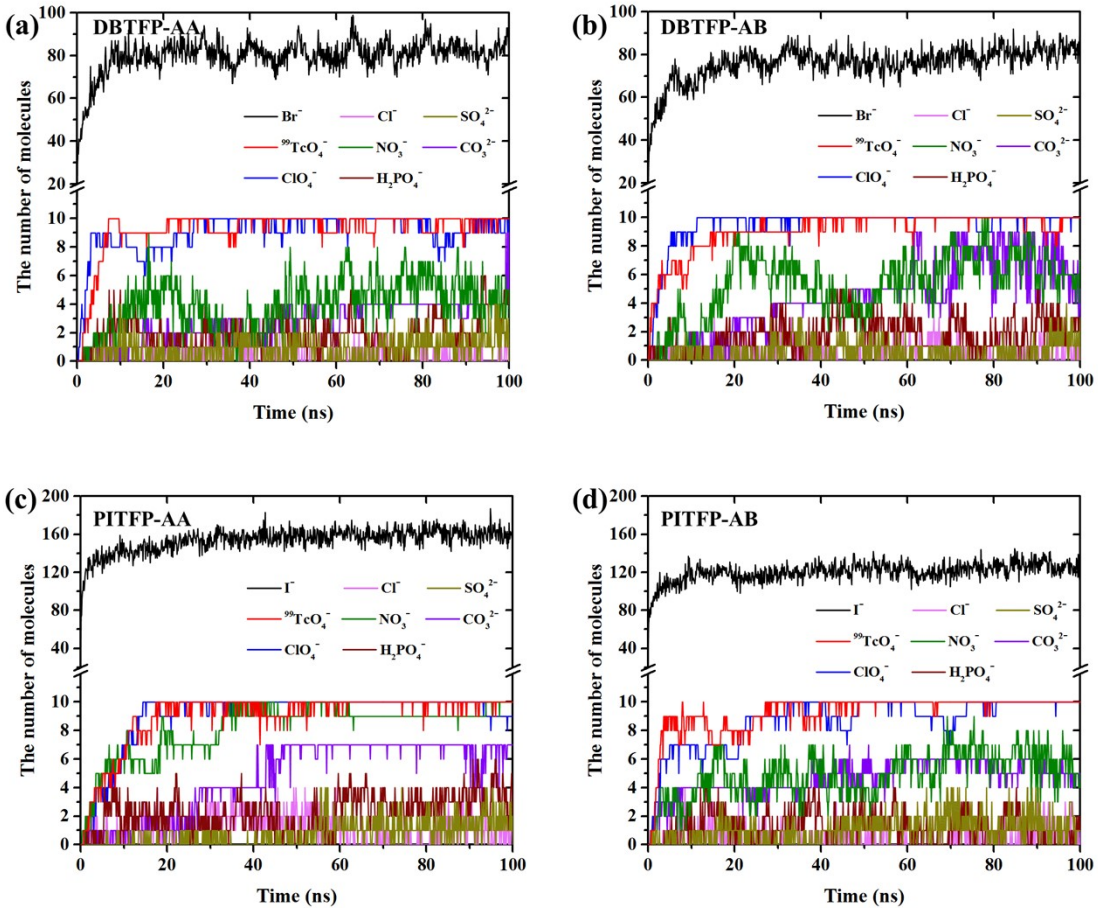

Fig. S12. Time evolution of the amounts of desorbed Br^- (or I^-) and adsorbed TcO_4^- as well as competing anions in (a) DBTFP-AA, (b) DBTFP-AB, (c) PITFP-AA and (d) PITFP-AB.

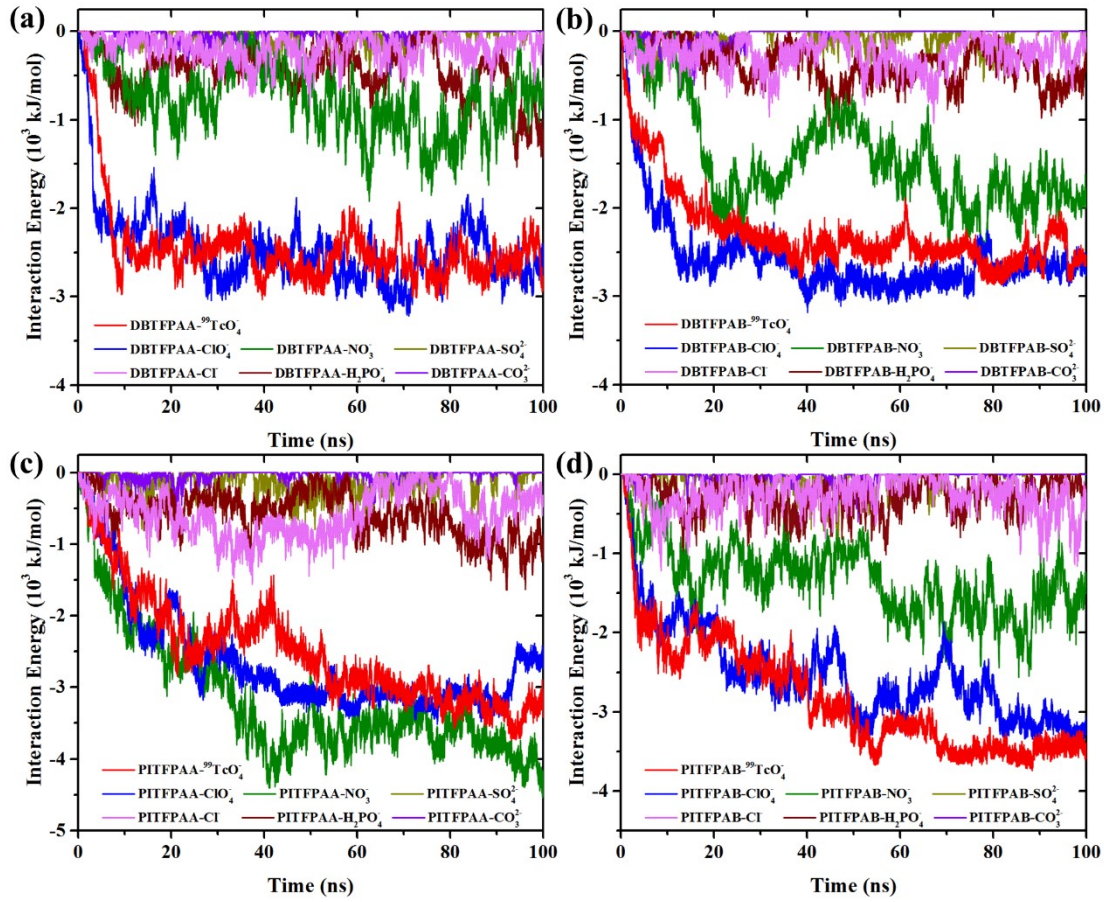

Fig. S13. The Coulomb interaction energies between (a) DBTFP-AA, (b) DBTFP-AB, (c) PITFP-AA as well as (d) PITFP-AB and anions.

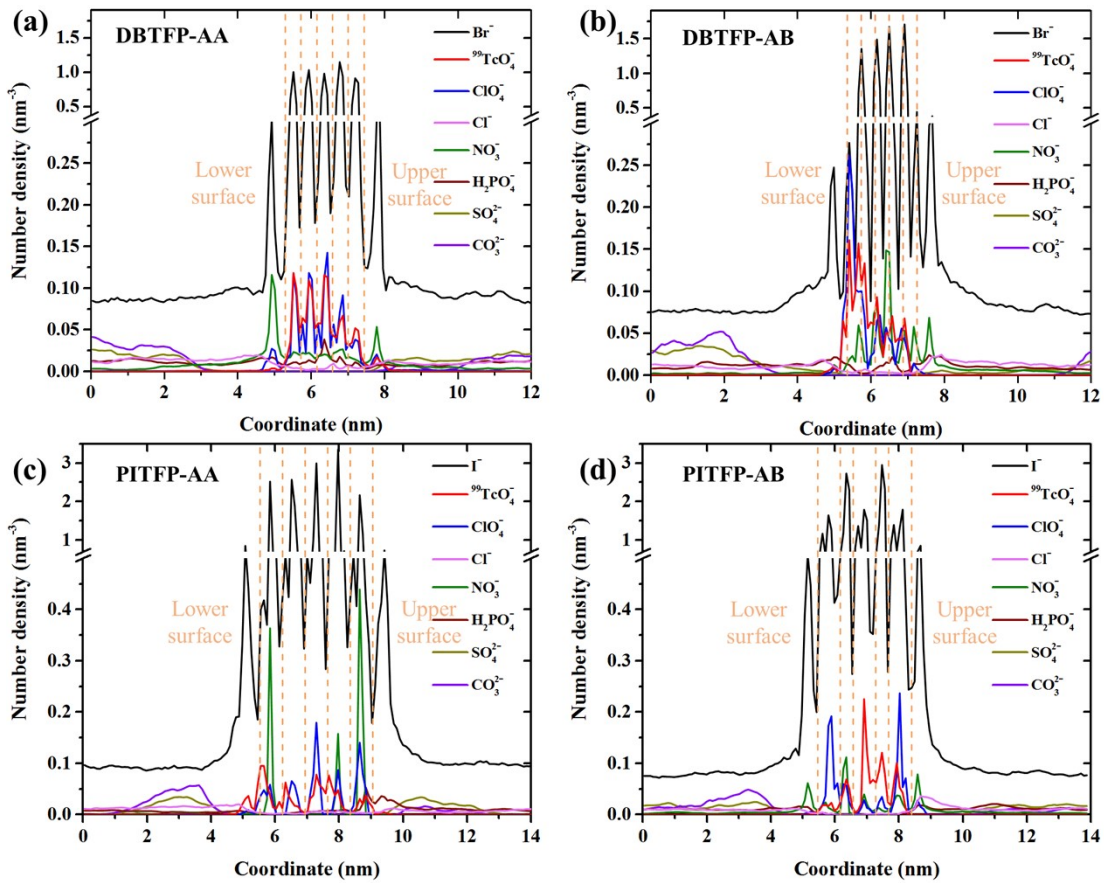

Fig. S14. The number densities of Br^- (or I^-), $^{99}TcO_4^-$ and competing anions in (a) DBTFP-AA, (b) DBTFP-AB, (c) PITFP-AA and (d) PITFP-AB. The orange dashed lines show the location of each layer.

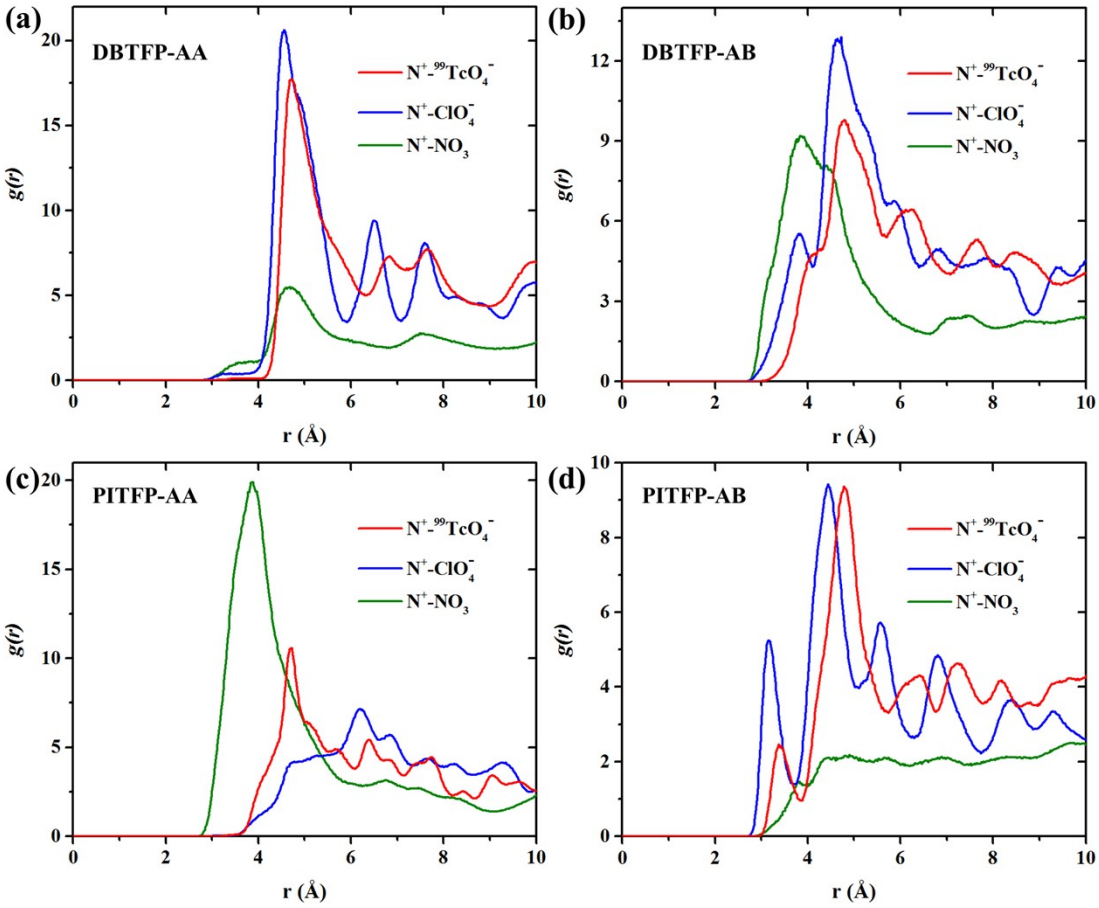

Fig. S15. The radial distribution functions (*g(r)*) of $^{99}TcO_4^-$ together with ClO_4^- and NO_3^- near the positively charged nitrogen atoms in (a) DBTFP-AA, (b) DBTFP-AB, (c) PITFP-AA and (d) PITFP-AB.

1. S. Mitra, S. Kandambeth, B. P. Biswal, A. Khayum M, C. K. Choudhury, M. Mehta, G. Kaur, S. Banerjee, A. Prabhune and S. Verma, Self-exfoliated guanidinium-based ionic covalent organic nanosheets (iCONs), *Journal of the American Chemical Society*, 2016, **138**, 2823-2828.